



Shahid Chamran  
University of Ahvaz

# Journal of Applied and Computational Mechanics



Research Paper

## Convective Instability in Forchheimer-Prats Configuration with a Saturating Power-Law Fluid

Hanae El Fakiri<sup>✉</sup>, Hajar Lagziri<sup>✉</sup>, Abdelmajid El Bouardi, Mohammed Lhassane Lahlaoui

Energy Laboratory, Physics Department, Faculty of Sciences, Abdelmalek Essaadi University, Tétouan, 99350, Morocco

Received September 07 2023; Revised December 31 2023; Accepted for publication January 04 2024.

Corresponding author: H. El Fakiri (elfakiri.hanae-etu@uae.ac.ma)

© 2024 Published by Shahid Chamran University of Ahvaz

**Abstract.** The paper deals with the combined effect of non-Newtonian saturating fluid and horizontal flow rate on the thermal convection in a highly permeable, porous plane layer saturated with a power-law model. Asymmetric boundary conditions are assumed, with a cooled free surface at the top and a heated, impermeable, rigid wall at the bottom. The generalised Forchheimer equation is employed to model the power-law fluid movement. Convection cells emerge in the power-law fluid because of vertical temperature gradient imposed by the thermal boundaries. The onset of this scenario can be studied using linear stability theory, which leads to an eigenvalue problem. The latter is solved either numerically, employing shooting schemes, or analytically, using one-order Galerkin approach. The present study is considered an extension of the classical Prats problem. When the Peclet number, which defines the flow rate, is negligible, the configuration switches to the special case of Darcy-Rayleigh instability. The results show that the form drag exhibits a stronger stabilizing influence in shear-thinning fluids compared to shear-thickening and Newtonian ones since the saturating fluid is described by the power-law model. This scenario appears in the specific range of the Peclet number. In general, this investigation can be used to understand the heat transfer process in subsurface hydrocarbon reservoirs where the fluid may exhibit non-Newtonian behaviour.

**Keywords:** Non-Newtonian fluids, porous media, Darcy-Forchheimer flow, Thermal instability, Horizontal throughflow.

### 1. Introduction

From the standpoint of numerous authors, Darcy's law is one of the simplest basic models used to define fluid motion (Newtonian or non-Newtonian) in weakly permeable porous-Bénard problems [1-4]. The Darcy equation is valid as long as the upper limit of the Reynolds number is similar to Stokes flow. This limitation does not emphasise the departure of the flow from a laminar to a transition or turbulence regime but rather the increasing effect of inertia on the microscopic level. In other words, despite having a wide range of applicability, Darcy's model fails to account for the quadratic term of velocity that expresses the nonlinear laminar regime. The deviation from the Darcy model becomes even more prominent in situations like multi-permeability and fractured systems in oil reservoirs, or for highly porous media and compressible fluids [5, 6]. To address this deviation, a parameter called the Forchheimer coefficient or form drag number has been considered to indicate the presence of nonlinearity created by fluid inertia [7]. The application of the Forchheimer model as a momentum equation in the modelling of fluid flow in highly permeable porous systems is still not widely used in the investigation of convective instability, as there is a scarcity of papers on this topic. The first study carried out in this context was by He and Georgiadis [8], who assumed the pure Horton-Rogers-Lapwood configuration (HRL) under conditions of high permeability (form drag), internal heating, and thermal dispersion. Their findings revealed that the combined effects of these three mechanisms can trigger and influence the early development of convection, where a pair of sharp-nosed bifurcations can arise instead of the customary pitchfork bifurcation. Shivakumara et al. [9] analysed the unstable nature of buoyant flow in a highly permeable Prats configuration saturated with Oldroyd-B fluid using combined boundary conditions between an isothermal rigid wall and an adiabatic porous layer. It is shown that the increase in the form drag number and the retardation time of the viscoelastic fluid can, on one hand, slow the onset of instability, and on the other hand, decrease the critical wave number in both cases of the boundary conditions. The onset of buoyancy-driven instability in a vertical highly permeable porous slab sandwiched between two permeable and isothermal boundaries was investigated by Barletta et al. [10]. The results found by these researchers indicate that the form drag number has a drastic effect on the emergence of transverse rolls, as well as on the threshold values of the wave number. In addition to this work, Barletta et al. [11] have studied the impact of the form drag number on the Prats configuration, taking into consideration the viscous dissipation of the saturating Newtonian fluid. They observed that the form drag number affects the appearance of transverse or oblique rolls more than longitudinal ones. The working fluid mentioned in these papers belongs to either Newtonian or non-Newtonian behavior, viz., the viscoelastic model. Thermal convection or convective instability in non-Newtonian fluid-saturated porous media has proven to have broad applications across various fields such as oil extraction, bioengineering, geophysics, and more [12]. For instance,



underground fluid reservoirs, especially those containing heavy oil and bitumen, can exhibit behavior identical to the power-law model.

The power-law model, in general, can transition from shear-thinning to Newtonian and then to shear-thickening fluid based on the strength of the applied shear stress. This characteristic makes it particularly appealing in research areas, especially in the context of convective instability in a porous structure. For more in-depth insights, Shenoy's book [13] offers a comprehensive review of the literature related to the modelling of power-law fluids saturating a porous matrix. The analysis of free and forced convection for power-law fluids in Shenoy's book was based on the generalised Darcy's equation developed by Christopher and Middleman [14].

Years later, Nield [15] demonstrated that applying linear stability theory to the power-law fluid saturating the classical problem of Horton-Rogers-Lapwood (HRL) can give rise to a singular mathematical problem when the rheological behavior of the fluid differs from the Newtonian one. According to Nield [15], this singularity can be avoided by assuming proportionality between the drag term highlighted in Darcy's equation for non-Newtonian fluids and the term  $|u|^{n-1}|u|$ , which is constituted by the power-law index  $n$  and the seepage velocity  $|u|$ . The buoyant flow of the power-law fluid under the effect of a vertical pressure gradient in the pure setup of HRL was considered by Barletta et al. [16]. Their outcomes display that the behavior of non-Newtonian fluid can accelerate the instability effects. This scenario occurs due to the growing dependence of the onset condition on the impact of the flow rate. The convective instability stemmed from the viscous dissipation of the power-law fluid in the Prats configuration with an insulating rigid lower boundary was investigated by Celli et al. [17]. They showed that the transverse rolls are the most unstable mode in shear-thinning fluid, while the longitudinal rolls are the most unstable mode for the shear-thickening one. Brandao et al. [18] have tackled the contribution of the permeable boundary conditions to the onset of instability of the power-law fluid saturating a porous layer that undergoes the effect of the vertical throughflow. The interesting point in this work was the transformation of the wave number from zero to non-zero values when the flow rate suppresses certain threshold values. This feature emerges in the three types of the fluid, namely shear thinning, Newtonian, and shear thickening cases. The most common point among these papers is that the convective instability of the power-law fluid is only studied in a weakly permeable porous layer where the effect of fluid inertia is negligible.

The aim of the current work is to fill this gap by dealing with the effect of the form drag number, which mentions the fluid inertia on the onset of convection of the power-law fluid saturating a highly permeable porous layer and undergoing horizontal throughflow. According to the author's knowledge, the contribution of the form drag number (the Forchheimer number) to the emergence of thermal instability of the power-law fluid has not been investigated yet. A linear stability theory that encompasses a linearization process and a normal modes method is performed together with dimensionless analysis. Controlling the dimensionless numbers such as the form drag number and Peclet number can manipulate the onset condition of thermal instability. Numerical and analytical techniques are both invoked here to define the critical values and validate the correctness of the solution.

## 2. Mathematical Formulation

Let us deal with the convective instability in a highly permeable porous layer where the saturating fluid behaves as a power law model (PL). The horizontal porous plane is situated in between two different horizontal surfaces: an isothermal impermeable wall at the bottom layer and an isoflux open surface at the top one (see Fig. 1). Uniform heat flux is assumed to cool the system by removing the heat and causing the vertical temperature gradient. The gravity force  $g$  is supposed to be perpendicular to the velocity of the flow and contrasted with the  $z$  direction. The momentum equation of the PL fluid is defined following a Forchheimer model proposed by Shenoy [13]. The Oberbeck–Boussinesq theory that manages the change of the density at the buoyancy forces is introduced beside the one energy equation Model. The set of equations written for this configuration is:

$$\nabla^* \cdot \mathbf{u}^* = 0, \quad (1a)$$

$$\frac{\eta}{\bar{K}} |\mathbf{u}^*|^{n-1} \mathbf{u}^* + \frac{C_F \rho}{\sqrt{K}} |\mathbf{u}^*| \mathbf{u}^* = -\nabla P^* + \rho g \beta (T^* - T_0), \quad (1b)$$

$$\sigma \frac{\partial T^*}{\partial t^*} + \mathbf{u}^* \cdot \nabla^* T^* = \alpha \nabla^{*2} T^*. \quad (1c)$$

$$z^* = 0: w^* = 0, \quad T^* = T_0, \quad (1d)$$

$$z^* = L: \frac{\partial w^*}{\partial z^*} = 0, \quad q = -\lambda_e \frac{\partial T^*}{\partial z^*}. \quad (1e)$$

where  $\mathbf{u}^*$  is the velocity components,  $(x^*, y^*, z^*)$  are the Cartesian coordinates,  $t^*$  is the time,  $T^*$  is the temperature,  $P^*$  is the pressure,  $g$  is the gravitational acceleration,  $\rho$  is the density of the power law fluid,  $K$  is the permeability of the porous structure,  $\beta$  is the thermal volumetric expansion coefficient,  $\eta$  is consistency index,  $n$  is the rheological behavior of the fluid,  $\alpha$  is thermal diffusivity,  $\lambda_e$  is the thermal conductivity,  $q$  is the uniform heat flux, and  $C_F$  is the dimensional Forchheimer coefficient.

Otherwise, for power-law fluids, for non-Newtonian power-law fluids, the modified permeability  $\bar{K}$  can be formulated using the following equation [14, 19]:

$$\bar{K} = \frac{1}{2C_t} \left( \frac{n\phi}{3n+1} \right)^n \left( \frac{50K}{3\phi} \right)^{(n+1)/2}. \quad (2)$$

Christopher and Middleman [14] considered the tortuosity factor  $C_t$  as a parameter independent of the power law index and equal to 25/12. Besides letting  $n = 1$  in Eq. (2) renders  $\bar{K}$  tends to  $K$  and  $\eta$  to  $\mu$  which leads Eq. (1b) to coincide with the standard form of the Forchheimer equation.



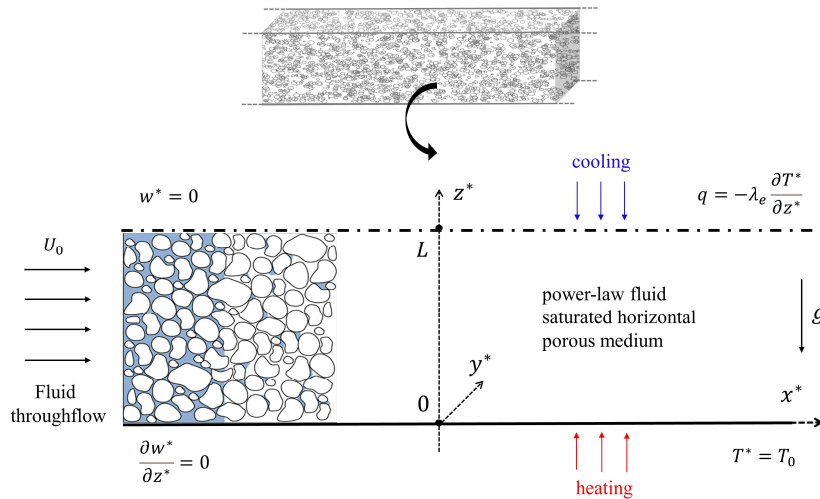


Fig. 1. Configuration of the system.

2.1. Non-dimensional analysis

One may highlight the dimensional variables rescaled by quantities symbolized without asterisks in the following manner:

$$u^*(u^*, v^*, w^*) = \frac{\alpha}{L} u(u, v, w), \quad t^* = \frac{L}{\sigma \alpha} t, \quad T^* = T \Delta T + T_0, \quad (x^*, y^*, z^*) = L(x, y, z). \tag{3}$$

The curl operator and the dimensionless process are both applied in Eqs. (1) which provides the given form:

$$\nabla \cdot \mathbf{u} = 0, \tag{4a}$$

$$\nabla \times (|\mathbf{u}|^{n-1} \mathbf{u} + G|\mathbf{u}|\mathbf{u}) = -R\nabla \times T\mathbf{e}_z, \tag{4b}$$

$$\frac{\partial T}{\partial t} + \mathbf{u} \cdot \nabla T = \nabla^2 T. \tag{4c}$$

$$z = 0: w = 0, T = 0, \tag{4d}$$

$$z = 1: \frac{\partial w}{\partial z} = 0, \frac{\partial T}{\partial z} = -1. \tag{4e}$$

The form-drag number  $G$ , and the Darcy-Rayleigh number  $R$  are the resulting non-dimensional parameters obtained through the last procedure in addition to other physical numbers whose expressions noted by:

$$R = \frac{\rho \beta g \bar{K} \Delta T L^n}{\eta \alpha^n}, \quad \sigma = \frac{\phi \rho_f c_f + (1 + \phi) \rho_s c_s}{\rho_f c_f}, \quad G = \frac{\rho C_F \bar{K} L^{n-2}}{\sqrt{K} \eta \alpha^{n-2}}, \quad Q = \frac{U_0 L}{\alpha}, \quad \Delta T = \frac{q L}{\lambda_e}, \quad \alpha = \frac{\lambda_e}{\rho_f c_f}, \quad \lambda_e = \phi \lambda_f + (1 - \phi) \lambda_s. \tag{5}$$

According to the Reynolds number defined in the literature [14], the deviation from the Darcy to the non-Darcy flow (form drag effect) for Newtonian fluid is not just based on permeability but is also related to other physical quantities such as viscosity and velocity. For the power law model, one may adopt the same scenario by using  $\eta$  instead of  $\mu$  and  $\bar{K}$  rather than  $K$  which can yield:

$$Re_{\bar{K}, \eta} = \frac{\rho \sqrt{\bar{K}} |u|^{2-n}}{\eta}. \tag{6}$$

Following Eq. (6), the form drag effect can take place only if the permeability is sufficiently high. In order to attain this value, several parameters should be fixed such as the consistency index  $\eta$ , the power law index  $n$ , and the maximum velocity present in the flow area.

2.2. Steady state

We assume a steady, parallel, and uniform flow with dimensional velocity  $U_0$  at the direction of the  $x$ -axis noted as:

$$\mathbf{u}_B = (Q, 0, 0), \tag{7a}$$

where  $Q$  is the classical Péclet number and is defined in Eqs. (5). Moreover, the temperature profile corresponds to the solution of the dimensionless Eqs. (4) is written as:

$$T_B(z) = 1 - z. \tag{7b}$$

Here the index  $B$  signifies the basic solution.



### 3. Linear Stability Analysis

Linear Stability theory allows for decomposing the solution into two different parts: The first part is for the base flow (conductive solution), and the second one is for the disturbance whose amplitude  $\varepsilon$  is assumed to be infinitesimally small. Therefore, we can write that:

$$\mathbf{u} = \mathbf{u}_b + \varepsilon \tilde{\mathbf{U}}, \quad v = v_b + \varepsilon \tilde{V}, \quad w = w_b + \varepsilon \tilde{W}, \quad T = T_b + \varepsilon \tilde{\theta}. \quad (8)$$

Substituting Eqs. (8) into the system of Eqs. (4), neglecting all the nonlinear terms and taking into account Eqs. (7) brings about linearized perturbation equations:

$$\frac{\partial \tilde{U}}{\partial x} + \frac{\partial \tilde{V}}{\partial y} + \frac{\partial \tilde{W}}{\partial z} = 0, \quad (9a)$$

$$\frac{\partial^2 \tilde{U}}{\partial z^2} (n + G|Q|^{2-n}) + \frac{\partial^2 \tilde{W}}{\partial x^2} (1 + G|Q|^{2-n}) = -\frac{R}{|Q|^{n-1}} \frac{\partial \tilde{\theta}}{\partial x}, \quad (9b)$$

$$\frac{\partial \tilde{\theta}}{\partial t} + P \frac{\partial \tilde{\theta}}{\partial x} - \tilde{W} = \nabla^2 \tilde{\theta}, \quad (9c)$$

$$z = 0: \tilde{W} = 0, \tilde{\theta} = 0, \quad (9d)$$

$$z = 1: \frac{\partial \tilde{W}}{\partial z} = 0, \frac{\partial \tilde{\theta}}{\partial z} = 0. \quad (9e)$$

The transformation of the velocity components into two-dimensional flow required the stream function  $\psi$  given by:

$$\tilde{U} = Q^{1-n} \frac{\partial \psi}{\partial z}, \quad \tilde{W} = -Q^{1-n} \frac{\partial \psi}{\partial x}. \quad (10)$$

By employing Eqs. (10) into Eqs. (9) the system becomes in the form of stream function-temperature, namely:

$$\frac{\partial^2 \psi}{\partial z^2} (n + G|Q|^{2-n}) + \frac{\partial^2 \psi}{\partial x^2} (1 + G|Q|^{2-n}) = -R \frac{\partial \tilde{\theta}}{\partial x}, \quad (11a)$$

$$\frac{\partial \tilde{\theta}}{\partial t} + Q \frac{\partial \tilde{\theta}}{\partial x} - |Q|^{1-n} \frac{\partial^2 \psi}{\partial x^2} = \nabla^2 \tilde{\theta}, \quad (11b)$$

$$z = 0: \frac{\partial \psi}{\partial x} = 0, \tilde{\theta} = 0, \quad (11c)$$

$$z = 1: \frac{\partial^2 \psi}{\partial y \partial x} = 0, \frac{\partial \tilde{\theta}}{\partial z} = 0. \quad (11d)$$

Since the system is considered to be infinite, homogeneous, and isotropic in the  $x$  direction, with boundary conditions that are independent of  $x$ ,  $y$  and  $t$  we can seek the solutions for  $\psi$  and  $\tilde{\theta}$  in the form of Fourier modes, known as normal modes and defined as:

$$\psi(x, z, t) = if(z)e^{i(ax - \omega t)}, \quad (12a)$$

$$\tilde{\theta}(x, z, t) = h(z)e^{i(ax - \omega t)}. \quad (12b)$$

The amplitudes of the stream function and the temperature are symbolized by  $f(z)$ , and  $h(z)$ , respectively. The introduction of the modal form Eqs. (12) into the perturbed governing Eqs. (11) leads to:

$$f''(n + G|Q|^{2-n}) - a^2 f(1 + G|Q|^{2-n}) = -Rah, \quad (13a)$$

$$h'' - a^2 h + i\omega h + |Q|^{1-n} af = 0, \quad (13b)$$

$$z = 0: f = 0, h = 0, \quad (13c)$$

$$z = 1: f' = 0, h' = 0. \quad (13d)$$

The rescaled expression of  $\hat{\omega}$  can be summed up as:

$$\hat{\omega} = \omega - aQ \quad (14)$$

The complex angular frequency and the wave number are mentioned by the notation of  $\omega$  and  $a$ .



### 3.1. The principle of exchange of stabilities (PES)

Stationary convection can be demonstrated by going through the analytical calculation which consists in multiplying Eqs. (13a-13b) with the complex conjugate of  $\bar{f}$  and  $\bar{h}$  then integrating them by parts in the interval  $[0, 1]$  in the following manner:

$$(n + G|Q|^{2-n}) \int_0^1 |f'|^2 dz + a^2(1 + G|Q|^{2-n}) \int_0^1 |f|^2 dz - Ra \int_0^1 \bar{f}h dz = 0 \tag{15}$$

$$\int_0^1 |h'|^2 dz + (a - i\hat{\omega}) \int_0^1 |h|^2 dz - a|Q|^{1-n} \int_0^1 \bar{h}f dz = 0. \tag{16}$$

Since  $(a, G, Q, n, R)$  have real values with  $\int_0^1 \bar{f}h dz \in \Re$ , and  $\int_0^1 \bar{h}f dz \in \Re$ , the real and imaginary part of Eq. (16) must be equal to zero. These requirements can be met only if the imaginary part:

$$\hat{\omega} \int_0^1 |h|^2 dz = 0 \tag{17}$$

The satisfaction of Eq. (17) can occur under two scenarios: either  $h = 0$  or  $\hat{\omega} = 0$ . We can exclude the first possibility since it leads to no perturbation solution  $f = h = 0$  and can keep the second one  $\hat{\omega} = 0$  whose negligible behavior seems more realistic. By combining this finding with Eq. (14), we obtain  $\hat{\omega} = aQ$  which gives rise to a similar result of Celli et al. [20]. This outcome confirms that the disturbance pattern travels at the same velocity as the basic state.

## 4. Analytical and Numerical Analysis

After the fulfillment of the PES two distinct approaches are proposed to solve the eigenvalue problem outlined in Eq. (13): the numerical solver FindRoot (shooting scheme) from Mathematica software and the analytical one-term Galerkin method. A concise description of each approach is provided below with a detailed explanation.

### 4.1. Analytical approach

The one term Galerkin method ( $N = 1$ ) is sufficient for achieving accurate results according to Tables 1 and 2. Therefore, the perturbed functions can be developed in the following trigonometric form (see for instance Finalyson [21]):

$$f(z) = A \sin\left(\frac{\pi}{2}z\right), \quad h(z) = B \sin\left(\frac{\pi}{2}z\right). \tag{18}$$

where the coefficients  $A$  and  $B$  are mentioned as non-complex constants. The trial functions defined in Eq. (18) satisfy the boundary conditions noted in the two last lines of Eq. (13). One may substitute Eqs. (18) into Eqs. (13) then multiply the resulting equations by  $\sin(\pi z/2)$  and integrate them in the interval  $[0,1]$  which results in a set of equation that possesses trivial solutions if:

$$\begin{pmatrix} -\left[\frac{\pi^2}{4}(n + G|Q|^{2-n}) + a^2(1 + G|Q|^{2-n})\right] & aR \\ a|Q|^{1-n} & -\left(\frac{\pi^2}{4} + a^2\right) \end{pmatrix} = 0 \tag{19}$$

The null determinant of the system provides a clear formula for the Darcy-Rayleigh number  $R$  defined as:

$$R = \frac{\left(\frac{\pi^2}{4}(n|Q|^{n-1} + G|Q|) + a^2(|Q|^{n-1} + G|Q|)\right)\left(\frac{\pi^2}{4} + a^2\right)}{a^2}. \tag{20}$$

Equation. (20) permits us to draw the neutral curves by varying values of  $n, G$ , and  $Q$ . Moreover, one may also directly deduce  $R_c$  and  $a_c$  by deriving Eq. (20) with respect to  $a$  which yield:

$$R_c = \frac{(\sqrt{GQ^2 + Q^n} + \sqrt{GQ^2 + nQ^n})^2 \pi^2}{4Q}, \quad a_c = \frac{(GQ^2 + nQ^n)^{1/4} \pi}{2(GQ^2 + Q^n)^{1/4}}. \tag{21}$$

The expression of  $R_c$  and  $a_c$  reported in Eq. (21) serve to determine directly at which buoyancy driven instability onset in the medium. A straightforward expression of  $R_c$  and  $a_c$  can be concluded for some special cases such as Darcy-Rayleigh convection [22, 23], Prats flow [24] and absolute pseudoplastic case. These scenarios can occur only if certain conditions are imposed as we will see in the forthcoming sections.

#### 4.1.1. The Darcy-Rayleigh problem (DR)

The nonexistence of the horizontal flow rate ( $Q \rightarrow 0$ ) leads the fluid to have a motionless basic state. This limiting case becomes akin to the DR problem which can be called also by Horton-Rogers-Lapwood instability [22, 23]. The boundary conditions assumed for this special case differ from the customary configuration since the open surface is considered. Under this circumstance, one may get from Eq. (20) the following critical values:

$$\begin{cases} \lim_{|Q| \rightarrow 0} R_c = +\infty, & \text{Shear thinning fluids } (n < 1), \\ \lim_{|Q| \rightarrow 0} R_c = 0, & \text{Shear thickening fluids } (n > 1), \\ \lim_{|Q| \rightarrow 0} R_c = \pi^2. & \text{Newtonian fluids } (n = 1). \end{cases} \tag{22}$$



**Table 1.** Values of  $R_c$  and  $a_c$  for  $n = 1$  and  $G = Q = 0$ .

Methods	$R_c$	$a_c$
Nield [25]	9.86960	1.57080
Wilkes [26]	9.86960	1.57081
First order Galerkin	9.86960	1.57079
Shooting scheme	9.86960	1.57079

**Table 2.** Values of  $R_c$  and  $a_c$  for  $G = 0$  and  $G = 0.05$  are calculated by two different methods: shooting scheme (SS) and First order Galerkin method (FGM).

G = 0				
n	$a_c$ (FGM)	$R_c$ (FGM)	$a_c$ (SS)	$R_c$ (SS)
0.1	0.883323689	2.290735017	0.883323689	2.290735016
0.5	1.320877	5.084475177	1.320877	5.084475175
1	1.570796327	9.869604403	1.570796326	9.869604398
1.5	1.738371894	17.27090839	1.738371894	17.27090838
2	1.868002168	28.762135	1.868002168	28.76213499
G = 0.05				
n	$a_c$ (FGM)	$R_c$ (FGM)	$a_c$ (SS)	$R_c$ (SS)
0.1	1.101196274	3.490147249	1.101196274	3.490147248
0.5	1.360016673	6.096276904	1.360016672	6.096276901
1	1.570796327	10.85656484	1.570796326	10.85656484
1.5	1.72872492	18.26748419	1.72872492	18.26748419
2	1.856782428	29.77797896	1.856782428	29.77797895

Equation (22) results from evaluating the value of  $R_c$ , defined in Eq. (21), when  $Q$  approaches zero. This yields the following conclusions: For shear-thinning fluids ( $n < 1$ ), the system remains linearly stable in the Darcy-Rayleigh problem as the apparent viscosity approaches infinity at vanishing  $Q$ . This signifies the system shows a strong resistance to perturbations. In contrast, a linear instability arises in shear-thickening fluids ( $n > 1$ ), meaning a small influence of buoyancy forces can trigger convection due to the weakness of the apparent viscosity. Finally, the well-known values at which instability commences in the Darcy-Rayleigh problem  $R = \pi^2$  is obtained for Newtonian case, see Table 1.

**4.1.2. Limiting case of absolute pseudoplasticity**

When a fluid has an extremely small power law index ( $n \rightarrow 0$ ), the expression of  $R_c$  as well as  $a_c$  can be evaluated analytically through Eqs. (21) in the follow form:

$$\lim_{n \rightarrow 0} R_c = \left( \frac{(\sqrt{1 + GQ^2} + \sqrt{GQ^2})\pi}{2\sqrt{Q}} \right)^2, \quad \lim_{n \rightarrow 0} a_c = \frac{\pi}{2} \left( \frac{GQ^2}{1 + GQ^2} \right)^{1/4}. \tag{23}$$

The assessment of  $R_c$  and  $a_c$  reported in Eq. (23) under different limits of  $G$  reveals that for a weakly permeable porous layer (as  $G$  approaches 0) and a highly permeable porous layer (as  $G$  approaches  $\infty$ ), one may encounter  $R_c = \pi^2 / 4Q$  with  $a_c = 0$  for the former limit, and  $R_c \rightarrow \infty$  with  $a_c = \pi / 2$  for the latter. In other words, in the Darcian regime ( $G = 0$ ), the behavior of the flow rate determines the increase or decrease in instability, whereas in the non-Darcian regime, linear stability occurs due to the dominance of drag forces. This aligns well with the findings presented in Fig. 9. The noteworthy point here is the emergence of the vanishing wave number case at  $G \rightarrow 0$ , implying that only unicellular flow patterns can exist in the perturbation fluid.

**4.1.3. Prats flow**

If we would like to recover the Prats flow [24] by neglecting the form drag ( $G \rightarrow 0$ ), in Eq. (21), the critical values for the onset condition can be redefined as:

$$\lim_{G \rightarrow 0} R_c = \left( \frac{(\sqrt{Q^n} + \sqrt{nQ^n})\pi}{2\sqrt{Q}} \right)^2, \quad \lim_{G \rightarrow 0} a_c = \frac{(n)^{1/4} \pi}{2}. \tag{24}$$

In the Darcian regime ( $G = 0$ ), the flow rate ( $Q$ ) becomes the key factor in controlling the variation of  $R_c$  in Eq. (24) for all three types of fluids. Comparatively, the wavenumber ( $a_c$ ) remains unaffected by  $Q$  in Eq. (24), which validates the results displayed in Figs. 6 to 8.

**4.2. Numerical solution**

The conjunction between the shooting scheme and the Runge-Kutta solver is one of the more popular numerical tools used for finding out the critical values as well as the marginal stability curves. In fact, the Runge-Kutta method can be applied only if we transform the differential equations into an initial value problem. To realize this operation, four conditions at  $z = 0$  must be completed in the corresponding manner:

$$z = 0 : f = 0, f' = S_1, h = 0, h' = 1. \tag{25}$$

Since the eigenvalue problem is considered homogeneous, the normalization condition  $h'(0) = 1$  has to be included. On the other hand, the introduction of the unknown constants  $S_1$ , in the initial condition is required in order to accomplish the needed number. This unknown is developed together with  $R$  from the shooting method and with the help of the boundary conditions expressed at  $z = 1$ . The numerical procedure of these two methods is performed by using Mathematica 10 Wolfram, Inc. Each of these techniques has its own function which is available in the software. The shooting method can be involved by the function of Find Root while the Runge-Kutta solver can be employed through the NDSolve function. The marginal stability curves  $R(a)$  can be obtained here only by giving certain values to the parameters  $Q, n, G$ , and  $a$ .



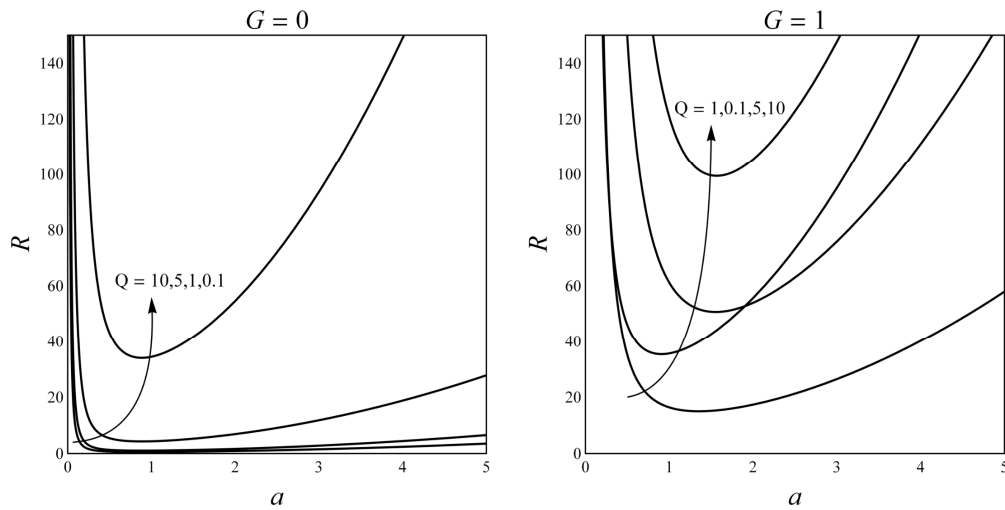


Fig. 2. Neutral plots  $R(a)$  for  $n = 0.1$ .

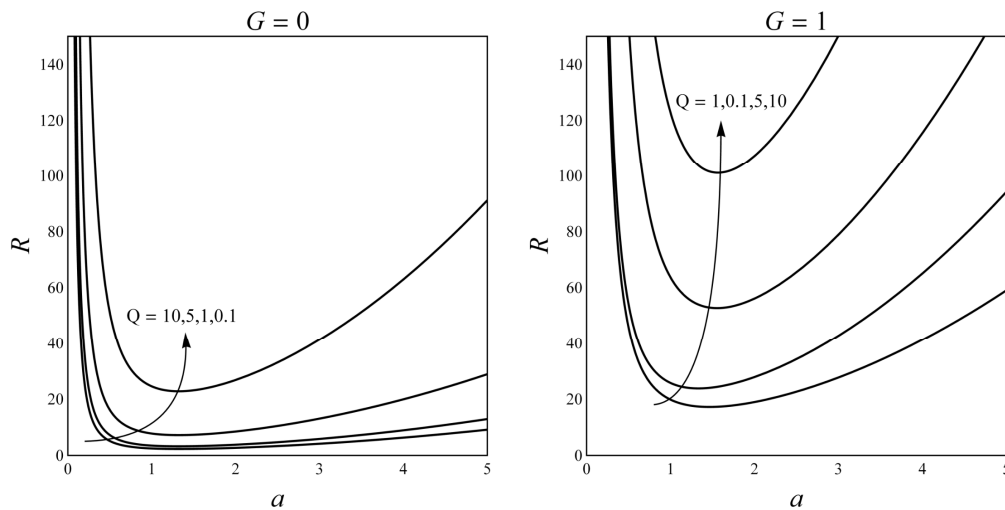


Fig. 3. Neutral plots  $R(a)$  for  $n = 0.5$ .

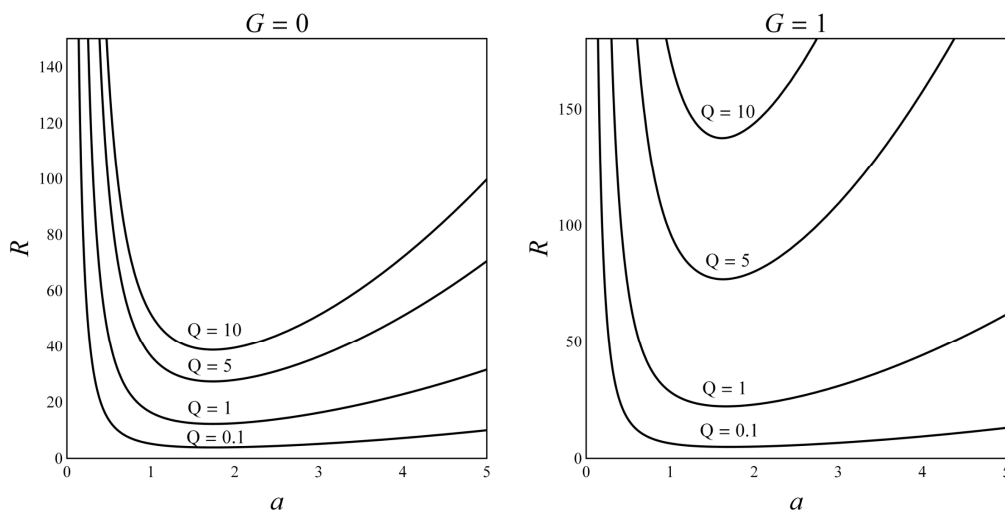


Fig. 4. Neutral plots of  $R(a)$  for  $n = 1.5$ .

4.2.1. Methods validation

The results of  $R_c$  and  $a_c$  generated by the techniques detailed in sections 4 and 5 are compared with those acquired by Nield [25] and Wilkes [26] under conditions of Newtonian fluid ( $n = 1$ ) with no flow rate and weakly permeable porous layer ( $Q = G = 0$ ). This study is carried out to validate the accuracy and the correctness of both methods against the literature. According to Table 1, an excellent agreement of 98.42% is demonstrated between the critical values developed by Nield [25] and Wilkes [26] and those



calculated by the first-order Galerkin method (FGM) and shooting scheme (SS). On the other hand, these two methods have also shown a good congruence between each other with no less than eight significant figures as provided in Table 2.

### 5. Outcomes and Discussions

This study investigates the dual contributions of the horizontal flow rate  $Q$  and the form drag  $G$  the emergence of thermal convection of the power-law fluid (whose viscosity changes with flow speed) in an isotropic homogeneous porous layer with asymmetric boundary conditions. The numerical and analytical results depicted in Figs. 2-9 enable us to understand how the parameters  $Q$  and  $G$  can control the thermal instability of underground fluid reservoirs containing power-law fluids like heavy oil and bitumen. These fluids exhibit a shear thickening and shear thinning behaviour against the applied shear stress. The flow rate  $Q$  which can be known as a Peclet number characterizes the effects of the applied shear stress at pore scales on a fluid, while the form drag  $G$  arises from the boundary layer detachment and its resulting wake. The onset of the thermal instability can be acknowledged through the determination of the minimum of the neutral curves drawn in Figs. 2-5 for different  $Q$  in the cases of Darcian regime ( $G = 0$ ) and non-Darcian regime ( $G = 1$ ). The area below the solid curves plotted in the parameter space ( $R, a$ ) represents stability, whereas the area above represents instability. The neutral curves display two uneven scenarios for a shear thinning fluid ( $n = 0.1, n = 0.5$ ): The first case shows a non-monotonic behaviour of  $R$  with respect to  $Q$  for the Darcy regime ( $G = 0$ ), while the second one exhibits a monotonic increase of  $R$  with  $Q$  for the non-Darcy regime ( $G = 1$ ). In other words, at negligible form drag ( $G = 0$ ), the apparent viscosity of the shear-thinning fluid becomes extremely strong at small Peclet number ( $Q$ ) and extremely weak at high Peclet number ( $Q$ ). This feature retards the trigger of thermal instability in the former case and accelerates it in the latter one, since the viscous forces have the lower hand at  $Q < 1$  and the upper hand at  $Q > 1$ . Conversely, the presence of form drag ( $G = 1$ ) prevents thermal instability from onsetting very easily at  $Q > 1$  which leads the system to reach a higher level of stability than the case of  $Q < 1$ . Physically speaking, it is well known that the drag forces slow the fluid movement because of the separation region created at the boundary layer caused by pressure differences. The appearance of this scenario hinders the dominance of buoyant forces during the fluid flow, which justifies the increase of the stability at  $Q > 1$ . Moreover, the impact of the form drag becomes increasingly apparent as the Peclet number strengthens. This elucidates why at  $Q < 1$  the instability behaviour quietly resembles that of  $G = 0$ . On the other hand, if we look at the shear thickening fluid ( $n = 1.5, n = 2$ ) one may notice a monotonic increase of  $R$  with respect to both  $Q$  and  $G$ . This corresponds to the parallel decrease in the apparent viscosity with the flow rate  $Q$  which gives rise to the opposite case of the previous one. In this context the thermal instability can quickly manifest when  $Q < 1$  at  $G = 0$  and  $G = 1$  as the fluid has a slow speed and less dominant viscous forces.

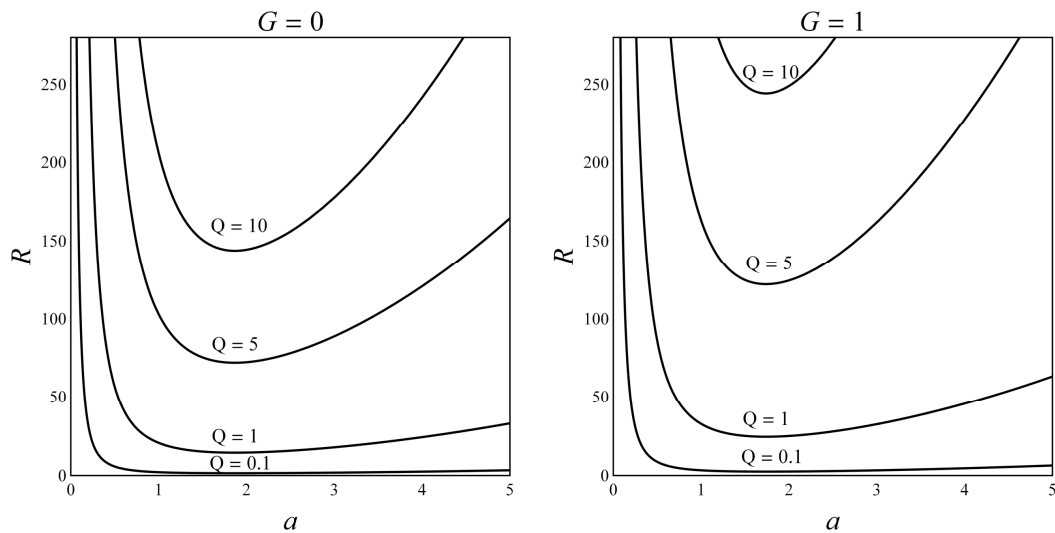


Fig. 5. Neutral plots of  $R(a)$  for  $n = 2$ .

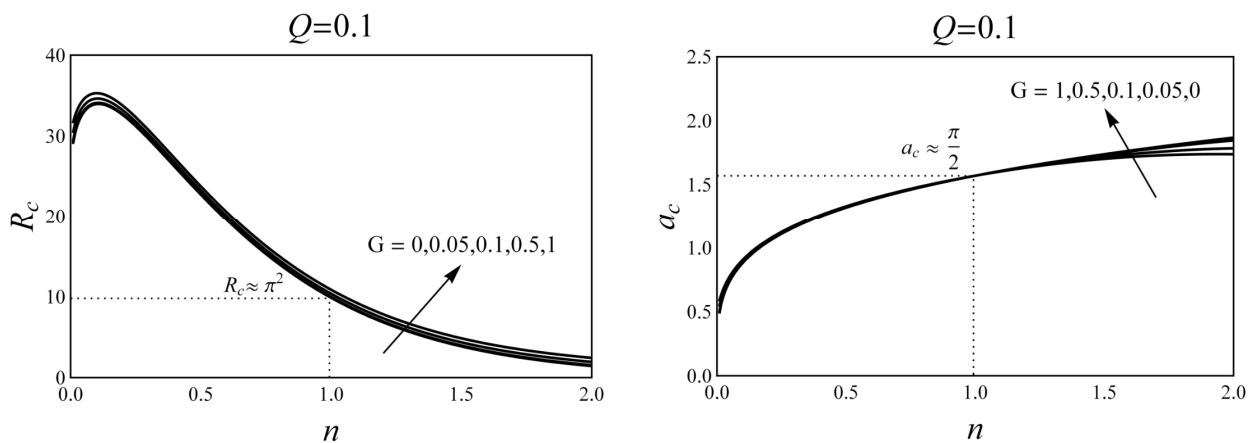


Fig. 6. Critical curves of  $R_c$  and  $a_c$  for fixed  $Q = 0.1, 1$ .





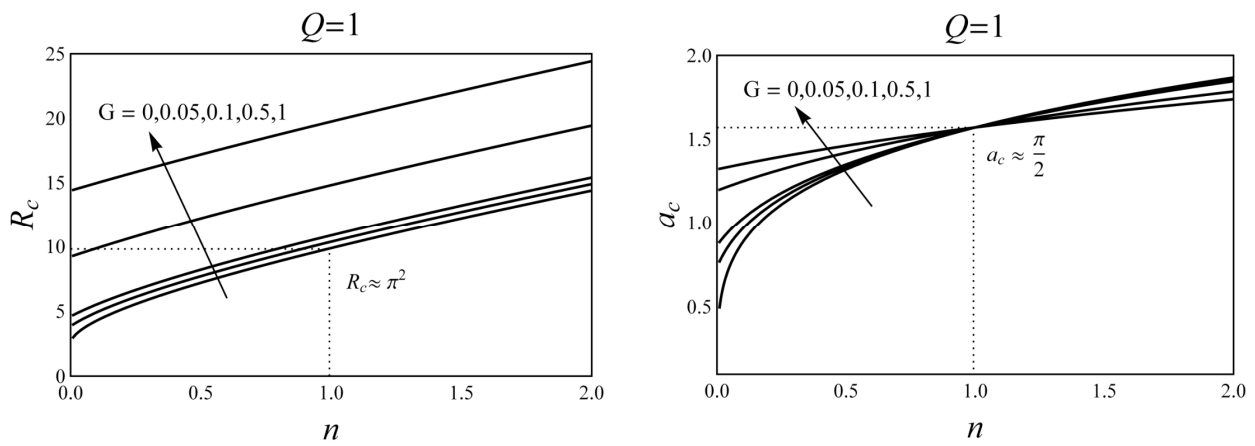


Fig. 6. Continued.

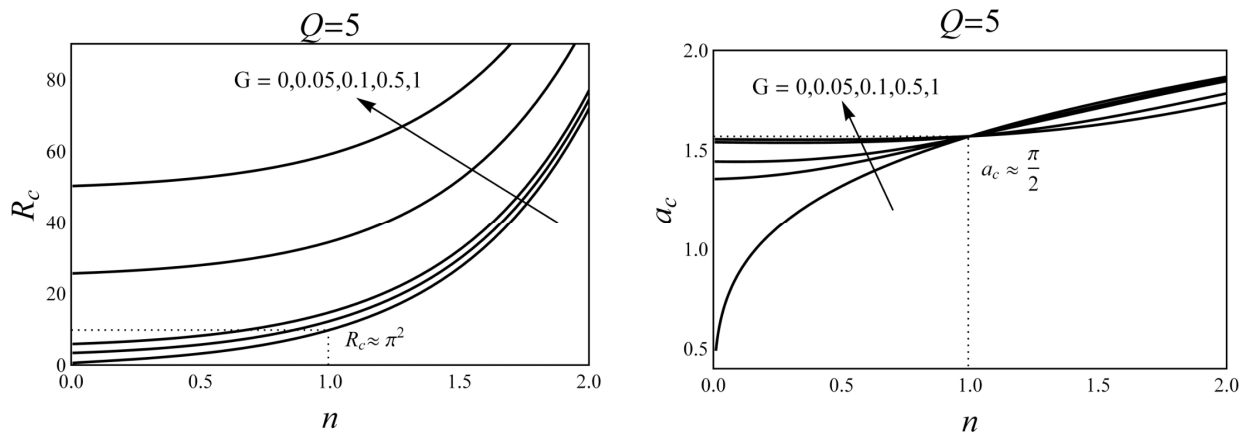


Fig. 7. Critical curves  $R_c$  and  $a_c$  for fixed  $Q = 5$ .

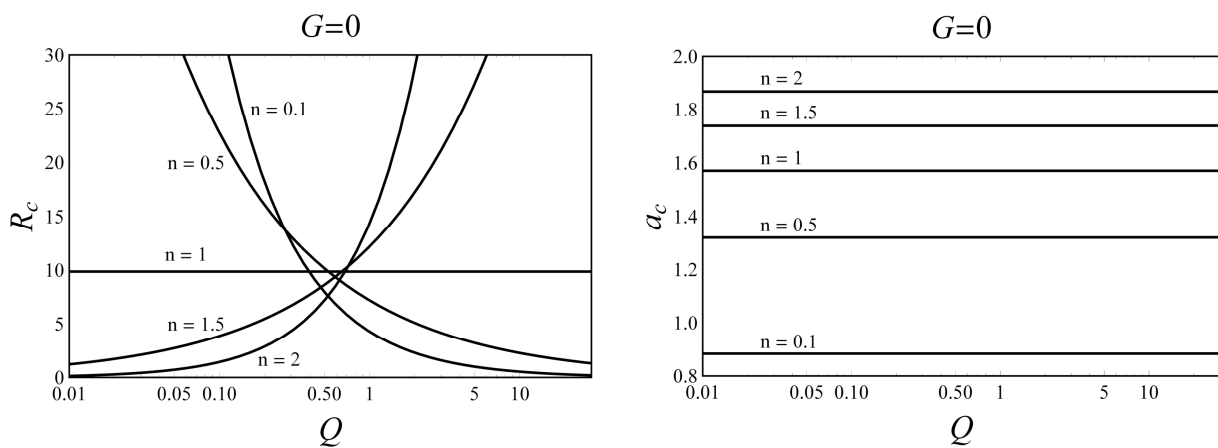


Fig. 8. Critical curves  $R_c$  and  $a_c$  for fixed  $G = 0, 0.1$ .

Figures 6, 7 and 8 present plots of the critical values of  $R$  and  $a$  against the power-law index  $n$  and  $Q$ . The dotted lines in Figs. 6 and 7 indicate the standard critical values determined as  $R_c = \pi^2$  and  $a_c = \pi^2 / 2$  by Nield [25] and Wilkes [26]. Both figures demonstrate that, at high Peclet numbers ( $Q$ ), thermal instability is difficult to induce in shear-thickening ( $n > 1$ ) and shear-thinning ( $n < 1$ ) fluids  $G > 0$ . For example, at  $Q = 5$  with  $G = 0.5$ , stability increases by 96.15% in shear-thinning fluid ( $n = 0.1$ ) and by 25.97% in shear-thickening fluid ( $n = 2$ ) when compared to Darcian flow. However, a rapid onset of thermal instability is observed at low Peclet numbers since the critical Darcy-Rayleigh number  $R_c$  grows by 2% for  $n = 0.1$  and 26.29% for  $n = 2$  at  $Q = 0.1$  and  $G = 0.5$ . This behavior aligns with the results discussed in the neutral curves as well as the one displayed in the Table 2. For a Newtonian fluid ( $n = 1$ ), the curve of  $R_c$  remains constant and linear with respect to the Peclet number ( $Q$ ) at  $G = 0$ , whereas it begins to diverge to infinity after  $Q = 1$  is surpassed at  $G = 0.1$ . This indicates that Newtonian fluids are more stable under conditions of  $G > 0$ , particularly in the case of  $Q > 1$ . Otherwise, if we look at the variation of  $a_c$  in both graphs (Fig. 2 and Fig. 8) one may conclude that the curves of the critical wave number remain constant with respect to the Peclet number  $Q$  in both fluids of shear-thinning and shear-thickening at Darcian regime  $G = 0$ .



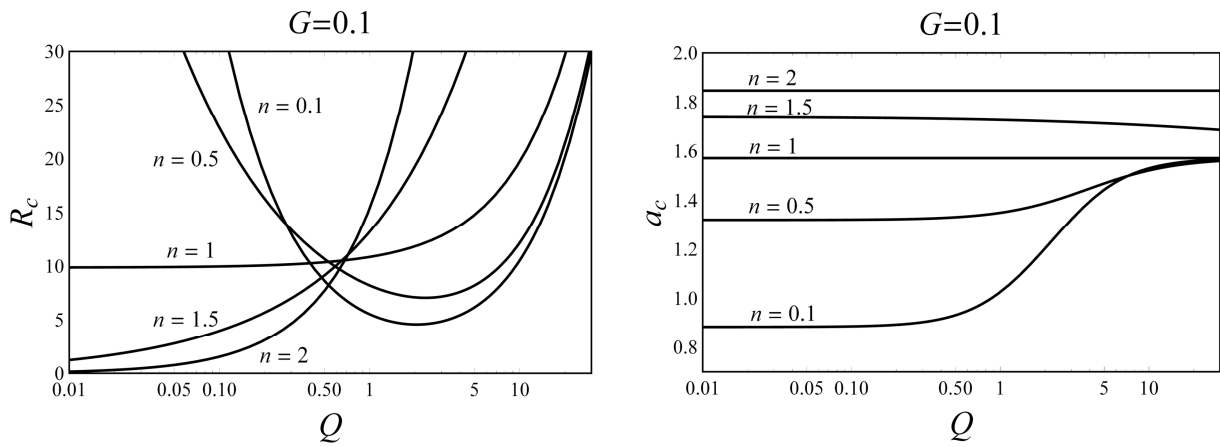


Fig. 8. Continued.

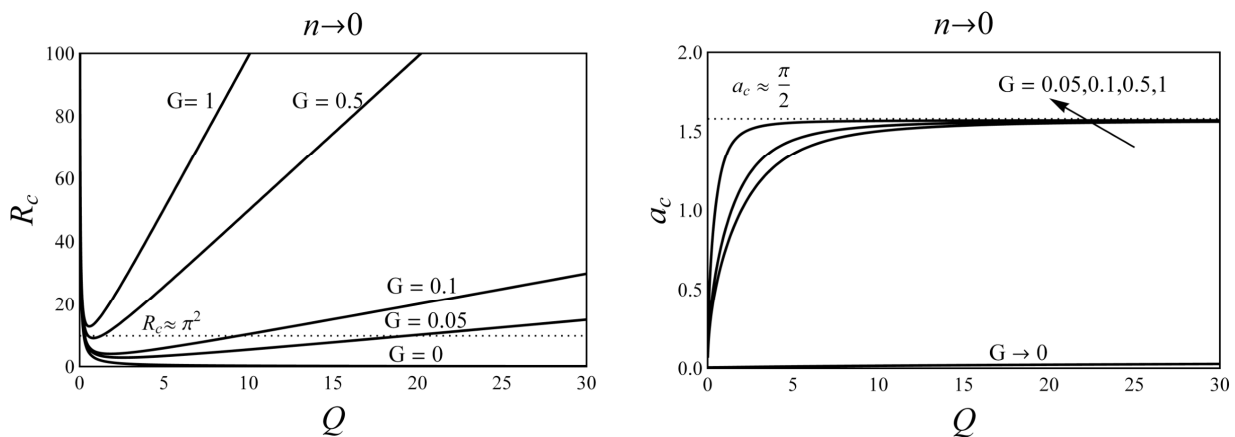


Fig. 9. Critical curves  $R_c$  and  $a_c$  for the limiting condition of  $(n \rightarrow 0)$

The deviation from this latter ( $G > 0$ ) drives the critical wavenumber to display a monotonic increase with the Péclet number until it reaches the standard value  $a_c = \pi^2 / 2$  for the Newtonian fluid. Thus, the growing of the Peclet number in this scenario rapid the arrival of the convective waves. Furthermore, it can be observed that the critical wave numbers slightly decrease as the form drag increases in a shear-thickening behavior. The understanding of the critical wave number can allow us to have a big picture of the cellular flow patterns of the perturbed fluid. According to the analysis above, the convective cells in the shear thickening case are more concentrated and smaller in size than the shear thinning one during the existence of the form drag. This in turn means a strong heat transfer process will be carried out in the porous layer. The special case of the absolute pseudoplastic model ( $n \rightarrow 0$ ) is mentioned in Fig. 9. Both plots of  $R_c$  and  $a_c$  with respect to  $Q$  and various values of  $G$  assure again the behavior displayed in Figs. 2 to 8. A special case of vanishing wave number appears for  $G = 0$ , implying the existence of a unicellular flow pattern. At  $G = 1$  and  $Q = 1$ , one may notice a 97.7% increase in the critical wave number  $a_c$  which drives the system to display more cells in the flow pattern. Broadly speaking, the occurrence of the form drag can enhance the stability of the shear thinning fluids which can facilitate many industrial operations such as the extraction of heavy oil or bitumen.

### 6. Conclusion

The contribution of form drag, horizontal flow rate, and fluid rheological behavior (Power-law model) to the initiation of thermal instability in a homogeneous isotropic porous layer was analyzed analytically by employing the first-order Galerkin method and numerically by adopting shooting schemes. The study encompasses the start of instability in three types of fluids: shear-thickening, Newtonian, and shear-thinning. Analytical and numerical outcomes were obtained for  $G = 0$  (Darcian regime) and  $G > 0$  (non-Darcian regime or Forchheimer regime), showing that the combined presence of form drag  $G$  and strong flow rate  $Q$  acts to suppress the early development of convective patterns for shear-thinning fluid more than its counterparts (Newtonian and shear-thickening). For instance, increasing the form drag  $G$  from 0.05 to 1 in the case of shear-thinning behavior ( $n = 0.5$ ) can yield an increase in  $R_c$  at flow rates  $Q = 5$  by 89.13%. Conversely, the value of  $R_c$  can be increased for shear-thickening fluid ( $n = 1.5$ ) by 61.23%, and for Newtonian one ( $n = 1$ ) by 79.18%. The variation of  $a_c$  also exhibits an increase in the presence of form drag for shear-thinning fluids, but a decrease for shear-thickening fluids. The special case of a vanishing wavenumber appeared at the special case of absolute pseudoplastic ( $n \rightarrow 0$ ), where it displays one convective cell pattern in Darcian regime and a multicellular flow pattern in non-Darcian one. Thus, controlling the form drag  $G$  affords us the capability to either delay or accelerate the buoyancy effect within the power law model. These findings can greatly aid in the formulation of extraction strategies targeting heavy oil and bitumen reservoirs, particularly in regions marked by the presence of high-permeability channels or fractures.

### Author Contributions

H. El Fakiri prepared the research conceptualization, developed the research methodology, conducted the formal analysis, developed the mathematical modeling, examined the theory validation, and write the original draft. H. Lagziri prepared the research



conceptualization, developed the research methodology, conducted the formal analysis, developed the mathematical modeling, examined the theory validation, and write the original draft. A. El Bouardi reviewed, edited the writing and provided supervision. Mohamed L. Lahlaoui reviewed, edited the writing and provided supervision. All authors discussed the results, reviewed and approved the final version of the manuscript.

## Acknowledgments

Not applicable.

## Conflict of Interest

The authors declared no potential conflicts of interest concerning the research, authorship, and publication of this article.

## Funding

The authors received no financial support for the research, authorship, and publication of this article.

## Data Availability Statements

Not applicable.

## Nomenclature

Latin symbols		Greek letters	
$a$	Wavenumber of disturbances,	$\alpha$	Thermal diffusivity [ $\text{m}^2/\text{s}$ ],
$A$	Constant coefficient,	$\beta$	Thermal expansion coefficient [ $\text{K}^{-1}$ ],
$B$	Constant coefficient,	$\hat{\theta}$	Temperature disturbance,
$c$	Specific heat capacity [ $\text{J}/(\text{kg K})$ ],	$\rho$	Density [ $\text{kg}/\text{m}^3$ ],
$c_t$	Tortuosity factor,	$\lambda$	Thermal conductivity ratio [ $\text{W}/(\text{m}\cdot\text{K})$ ],
$C_F$	Forchheimer coefficient,	$\mu$	Dynamic viscosity [ $\text{Pa}\cdot\text{s}$ ]
$e_z$	Unit vector in the z-direction,	$\eta$	Consistency index,
$f(z), h(z)$	Eigenfunctions,	$\sigma$	Heat capacity ratio
$g$	Gravitational acceleration [ $\text{m}/\text{s}^2$ ],	$\Psi$	Dimensionless stream-function,
$G$	The form-drag number,	$\omega$	Rescaled angular frequency,
$i$	Complex number ( $i^2 = -1$ ),	$\hat{\omega}$	Shifted angular frequency,
$K$	Permeability [ $\text{m}^2$ ],	$\phi$	Porosity,
$\tilde{K}$	Modified permeability,	$\Delta T$	Reference temperature difference [ $\text{K}$ ],
$L$	Layer thickness [ $\text{m}$ ],	$\varepsilon$	Small parameter,
$P$	Pressure, [ $\text{Pa}$ ],	$\epsilon$	Dimensionless perturbation parameter.
$n$	Power law index,	Subscripts	
$q$	Uniform heat flux, [ $\text{W}/\text{m}^2$ ],	$B$	Basic state,
$Q$	Péclet number,	$c$	Critical value,
$R$	Darcy–Rayleigh number,	$e$	Effective value,
$\text{Re}_{\rho L}$	Reynolds number,	$f$	Fluid phase,
$t$	Time [ $\text{s}$ ],	$s$	Solid phase.
$T$	Temperature [ $\text{K}$ ],	Superscript	
$T_0$	Reference temperature [ $\text{K}$ ],	*	Dimensional quantity,
$u$	Dimensionless ( $u, v, w$ ),	'	Derivative with respect to z,
$\vec{U}$	Velocity disturbance vector ( $\vec{U}, \vec{V}, \vec{W}$ )	-	Complex conjugate.
$U_0$	Dimensional velocity flow,		
$(x, y, z)$	Cartesian coordinates.		


## References


- [1] Combarrous, M.A., Bories, S.A., Hydrothermal Convection in Saturated Porous Media, *Advances in Hydroscience*, 10, 1975, 231-307.
- [2] Nield, D.A., Bejan, A., *Convection in Porous Media*, Springer International Publishing AG, Cham, Switzerland, 2017.
- [3] Vafai, K., *Handbook of Porous Media*, CRC Press, Taylor & Francis Group, Boca Raton, 2015
- [4] Barletta, A., *Route to absolute instability in porous media*, Springer Nature, Cham, Switzerland, 2019.
- [5] Gérard, A., Genter, A., Kohl, T., Lutz, P., Rose, P., Rummel, F., The deep EGS (Enhanced Geothermal System) project at Soultz-sous-Forêts (Alsace, France), *Geothermics*, 35(5), 2006, 473–483.
- [6] Nie, R.S., Meng, Y.F., Jia, Y.L., Zhang, F.X., Yang, X.T., Niu, X.N., Dual porosity and dual permeability modeling of horizontal well in naturally fractured reservoir, *Transport in Porous Media*, 92(1), 2012, 213–235.
- [7] Nield, D.A., Joseph, D.D., Effects of quadratic drag on convection in a saturated porous medium, *Physics of Fluids*, 28, 1985, 995–997
- [8] He, X.S., Georgiadis, J.G., Natural convection in porous media: effect of weak dispersion on bifurcation, *Journal of Fluid Mechanics*, 216, 1990, 85-298
- [9] Shivakumara, I.S., Sureshkumar, S., Convective instabilities in a viscoelastic-fluid-saturated porous medium with throughflow, *Journal of Geophysics and Engineering*, 4(1), 2007, 104–115.
- [10] Barletta, A., Rees, D.A.S., On the onset of convection in a highly permeable vertical porous layer with open boundaries, *Physics of Fluids*, 31, 2019, 074106.



- [11] Barletta, A., Celli, M., Rees, D.A.S., Darcy-Forchheimer flow with viscous dissipation in a horizontal porous layer: onset of convective instabilities, *Journal of Heat Transfer*, 131(7), 2009, 072602
- [12] Chhabra, R.P., Richardson, J.F., *Non-Newtonian flow and applied rheology: Non-Newtonian Flow and Applied Rheology*, Elsevier, Oxford, 2008.
- [13] Shenoy, A., *Heat transfer to non-Newtonian fluids: fundamentals and analytical expressions*, Wiley-VCH, Germany, 2018.
- [14] Christopher, R.H., Middleman, S., Power-Law Flow through a Packed Tube, *Industrial & Engineering Chemistry Fundamentals*, 4(4), 1965, 422–426.
- [15] Nield, D.A., A Further Note on the Onset of Convection in a Layer of a Porous Medium Saturated by a Non-Newtonian Fluid of Power-Law Type, *Transport in Porous Media*, 88(2), 2011, 187–191.
- [16] Barletta, A., Storesletten, L., Linear instability of the vertical throughflow in a horizontal porous layer saturated by a power-law fluid, *International Journal of Heat and Mass Transfer*, 99, 2016, 293–302.
- [17] Celli, M., Barletta, A., Onset of convection in a non-Newtonian viscous flow through a horizontal porous channel, *International Journal of Heat and Mass Transfer*, 117, 2018, 1322–1330.
- [18] Brandão, P.V., Celli, M., Barletta, A., Alves, L.S.D.B., Convection in a Horizontal Porous Layer with Vertical Pressure Gradient Saturated by a Power-Law Fluid, *Transport in Porous Media*, 130(2), 2019, 613–625.
- [19] Federico, V.D., Pinelli, M., Ugarelli, R., Estimates of effective permeability for non-Newtonian fluid flow in randomly heterogeneous porous media, *Stochastic Environmental Research and Risk Assessment*, 24(7), 2010, 1067–1076.
- [20] Celli, M., Impiombato, A.N., Barletta, A., Buoyancy-driven convection in a horizontal porous layer saturated by a power-law fluid: The effect of an open boundary, *International Journal of Thermal Sciences*, 152, 2020, 106302.
- [21] Finalyson, B.A., *The Method of Weighted Residuals and Variational Principles*, Society for Industrial and Applied Mathematics, 2013.
- [22] Horton, C.W., Rogers, F.T., Convection Currents in a Porous Medium, *Journal of Applied Physics*, 16(2), 1945, 367–370.
- [23] Lapwood, E.R., Convection of a fluid in a porous medium, *Mathematical Proceedings of the Cambridge Philosophical Society*, 44(4), 1948, 508–521.
- [24] Prats, M., The effect of horizontal fluid flow on thermally induced convection currents in porous mediums, *Journal of Geophysical Research*, 71(20), 1966, 4835–4838.
- [25] Nield, D.A., Onset of Thermohaline Convection in a Porous Medium, *AGU Water Resources Research*, 4(3), 1968, 553–560.
- [26] Wilkes, K.E., Onset of Natural Convection in a Horizontal Porous Medium with Mixed Thermal Boundary Conditions, *Journal of Heat Transfer*, 117(2), 1995, 543–547.

## ORCID iD

Hanae El Fakiri  <https://orcid.org/0000-0001-8011-5294>

Hajar Lagziri  <https://orcid.org/0009-0006-4532-6735>



© 2024 Shahid Chamran University of Ahvaz, Ahvaz, Iran. This article is an open access article distributed under the terms and conditions of the Creative Commons Attribution-NonCommercial 4.0 International (CC BY-NC 4.0 license) (<http://creativecommons.org/licenses/by-nc/4.0/>).

**How to cite this article:** El Fakiri H., Lagziri H., El Bouardi A., Lahlaoui M.L. Convective Instability in Forchheimer-Prats Configuration with a Saturating Power-Law Fluid, *J. Appl. Comput. Mech.*, 10(2), 2024, 357-368. <https://doi.org/10.22055/jacm.2024.44741.4267>

**Publisher's Note** Shahid Chamran University of Ahvaz remains neutral with regard to jurisdictional claims in published maps and institutional affiliations.

